ARTICLE

Insights into the Carbon Balance for CO_2 Electroreduction on Cu using Gas Diffusion Electrode Reactor Designs

Received 00th January 20xx,
Accepted 00th January 20xx

DOI: 10.1039/x0xx00000x

Ming Ma,[a] Ezra L. Clark,[a] Kasper T. Therkildsen,[b] Sebastian Dalsgaard,[a] Ib Chorkendorff [a] and Brian Seger*,[a]

In this work, the carbon balance during high-rate CO_2 reduction in flow electrolyzers is rigorously analyzed. The CO_2 consumption at gas-diffusion electrodes due to electrochemical reduction and reaction with OH^- at the electrode-electrolyte interface leads to a substantial reduction in the volumetric flowrate of gas flow out of the electrolyzer, especially when highly alkaline electrolytes and elevated current densities are utilized, mainly owing to elevated pH at cathode/electrolyte interface. Without considering the CO_2 consumption, the Faradaic efficiencies for major gas products could be significantly overestimated during high current density CO_2 reduction conditions, particularly in the case of high pH electrolyte. In addition, a detailed carbon balance path is elucidated via a two-step procedure of CO_2 reaction with OH^- at cathode/electrolyte interface and subsequent CO_2 generation at anode/electrolyte interface caused by a relatively low pH in the vicinity of the anode. Based on the proposed two-step carbon balance path, a systemic exploration of gases released in anolyte reveals the transformation of a HCO_3- or OH^- catholyte to a CO_3^{2-} catholyte, which was further confirmed by pH measurement.

Introduction

The electrochemical conversion of CO_2 into fuels and valuable chemicals under mild conditions has gained significant interest as an attractive route for the storage of intermittent renewable energy and the utilization of the captured CO_2.[1–8] Over the past few decades, the focus of most CO_2 reduction research has concentrated on the development of selective, efficient and stable electrocatalytsts using traditional H-cell reactors filled with CO_2-saturated aqueous solutions.[9–12] Researchers have substantially reduced the overpotentials required for driving selective CO_2 reduction via tuning morphologies,[13,14] compositions,[15] facets[16,17] and oxidation states of catalysts[18]. Although impressive progress has been made on the improvement of catalytic performance, low CO_2 solubility in aqueous electrolyte and the thick mass–transfer boundary layer (> 50 µm) in H-cell lead to poor CO_2 mass transport to the surface of the catalysts,[19,20] which significantly limits the current densities, preventing the potential for practical applications.

To overcome the mass transport limitations, many attempts have focused on CO_2 reduction in flow-cell reactors with gas-diffusion electrodes (GDEs) which can offer a dramatically thinner mass–transfer boundary layer (~50 nm) that is a 3-order of magnitude decrease compared to that in H-cell reactors.[19–21] Based on the flow-cell configurations, electrocatalytic conversion of CO_2 has been widely performed in high concentration of neutral solutions (such as $KHCO_3$), demonstrating commercially-relevant current densities (> 100 mA/cm²).[22–26] For further improving catalytic selectivity of CO_2 reduction to desired products, high concentration of KOH solutions are becoming commonly employed in many studies of the GDE-type flow electrolyzers, owing to the high conductivity of OH^- and the stated reduction of activation energy barriers for CO_2 reduction influenced by OH^-.[21,26–31] However, it is well known that OH^- can react with CO_2 to form HCO_3^- or CO_3^{2-} according to below reactions:

$$OH^- + CO_2 \leftrightarrow HCO_3^- \quad \text{(pKa=7.8)} \quad (1)$$

$$OH^- + HCO_3^- \leftrightarrow CO_3^{2-} + H_2O \quad \text{(pKa=10.3)} \quad (2)$$

These reactions inherently lead to a change of electrolytes (such as anion species) over time, finally influencing the catalytic activity of CO_2 reduction. Recently, a slight decrease in current density was discovered during high-rate CO_2 reduction in 1 M KOH electrolyte, and this observation was reported to be linked to the transitioning of OH^- to CO_3^{2-} in electrolyte as the major charge carrier.[24] However, direct evidence of the anion species transformation at high-rate CO_2 reduction is still lacking.

In addition, there is a much more practical issue that comes with operating CO_2 reduction in basic conditions. Gaseous CO_2 reduction products are almost always quantified by measuring a concentration (i.e. via a GC) and monitoring the gas flow, as indicated in Equation S2 (catalytic selectivity calculation). While the incoming CO_2 flow can easily be measured by thermal mass flowmeters, variations in product streams (a mixture of different gases) after the reactor limit the available techniques for measuring outlet flows (mostly due to

[a] Department of Physics, Technical University of Denmark, 2800 Kgs. Lyngby, Denmark
[b] Siemens A/S, RC-DK SI, Diplomvej 378, 2800 Kgs. Lyngby, Denmark
† Footnotes relating to the title and/or authors should appear here.
Electronic Supplementary Information (ESI) available: [details of any supplementary information available should be included here]. See DOI: 10.1039/x0xx00000x

variations in thermal conductivity). At neutral pH electrolyte and low currents, it is reasonable to approximate outlet flows are equivalent to inlet flows since conversion rates are low (such as most of the cases in H-cell). However, basic solutions with the ability of capturing CO_2 via reaction with OH^- can significantly change the outlet flowrates. In addition, CO_2 conversion into C_2 gas products and liquid products at high reaction rates (i.e. high current densities) also affects the gas outlet flowrates. Thus, the measurement of outlet gas flow in high-rate CO_2 reduction plays an important role in calculation of Faradaic efficiency (FE) of gas products. However, currently the majority of work in high-rate CO_2 electroreduction[21–23,28,31–36] have not explicitly stated that their Faradaic efficiency calculations were based on the outlet gas flow from their reactor (exception for few research on CO_2 reduction to CO[37,38]). Therefore, to ensure results are not errantly reported in GDEs-type electrolyzers, it is critical to fundamentally understand the carbon balance and benchmark the evaluation of the catalytic selectivity (or FE) at high current densities. Herein, we demonstrate that the CO_2 consumption via the reaction with OH^- in flow electrolyzers (Figure 1a) can significantly reduce the total flowrate of gas outlet after electrolysis, especially in high concentration of alkaline solutions. In addition, this study also shows how the CO_2 consumption can affect evaluation of CO_2 reduction results and how electrolyte speciation dynamically changes at high current densities. In addition, this study provides new insights into the carbon balance of flow electrolyzers via systemically exploring carbon paths and the transformation of ion species in catholyte and anolyte.

Experimental Methods

Fabrication and characterization of Cu catalysts.

To obtain thin Cu electrocatalyst layers on GDEs with high purity, the Cu catalysts were deposited by a magnetron sputtering at an argon pressure of 2 mTorr. Figure 1a shows a typical scanning electron microscope image (SEM) of the Cu catalysts coated on the top of microporous carbon layers. In addition, the cross-sectional SEM image (Figure S1) indicates the Cu deposition rate was ~4 nm/min. Using this technique, we synthesized ~70 nm thick Cu catalyst layers on GDEs. To identify the phase of Cu catalysts, X-ray diffraction (XRD) measurements were conducted. The XRD patterns (Figure S4) show the PTFE[39] and carbon peaks derived from GDE substrates as well as the (111), (200), and (211) Cu peaks with the dominant (111) peak.

Electrocatalytic CO_2 reduction.

The electrochemical reduction of CO_2 was performed in a three-compartment flow electrolyzer, consisting of catholyte and anolyte flow compartments which are separated by an anion exchange membrane (AEM), and gas compartment which allows gases to flow in and out of the reactor, as shown in Figure 1a. The cathodic gas flow compartment was continuously fed with CO_2 at a constant flow rate (45 ml/min), and a part of CO_2 was converted into gas products, which directly vented into the gas-sampling loop of a gas chromatograph (GC) for periodical quantification (Figure 5S). Liquid-phase products formed during the CO_2 reduction were diluted in the given reservoir (catholyte and anolyte), and recycled until the test was finished. After completion of electrolysis, liquid-phase products

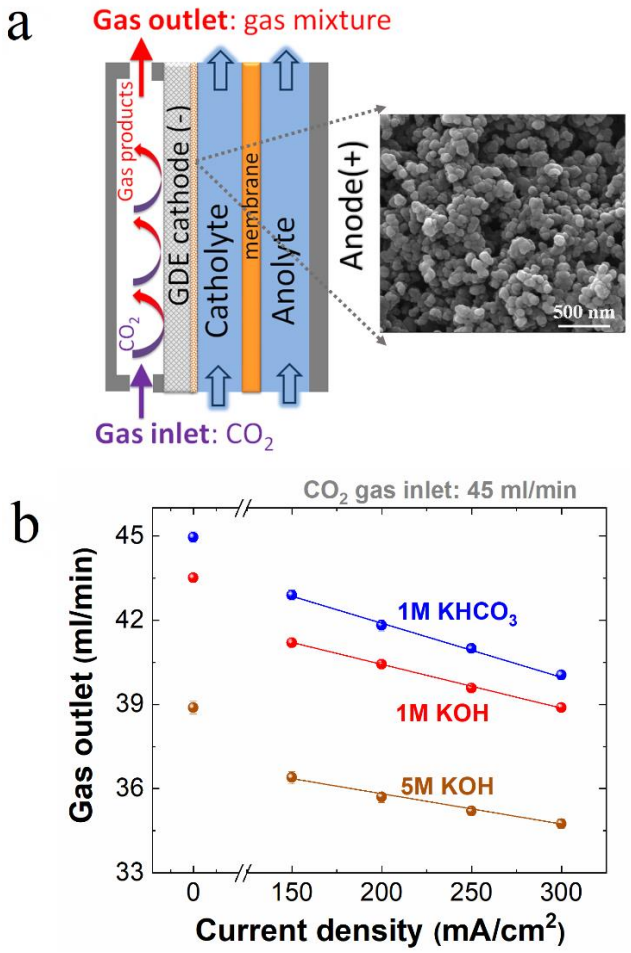

Figure 1. (a) Schematic illustration of three-compartment flow electrolyzers, and SEM image of Cu catalysts on GDEs. (b) Gas outlet flowrates from gas chamber after CO_2 reduction in 1 M $KHCO_3$, 1 M KOH and 5 M KOH, respectively.

were identified and quantified by a high-performance liquid chromatography (HPLC).

Results and Discussion

To verify the variation in gas flowrate between inlet and outlet, a volumetric flowmeter was used to monitor the outlet flow of our reactor (Figure 5S). Figure 1b shows the outlet flowrate as a function of current density (J) in 1 M $KHCO_3$, 1 M KOH and 5 M KOH, respectively. Without electrolysis (i.e. j=0 mA/cm^2), there is no obvious discrepancy in the flowrate between inlet and outlet in 1 M $KHCO_3$. In contrast, an evident decrease in the outlet flowrate was observed upon increasing the concentration of OH^- in electrolyte (J = 0 mA/cm^2), which stems from the enhanced CO_2 consumption rate through the reaction of CO_2 and OH^- in high pH solutions. As current densities increased, outlet flow gradually decreased in all the electrolytes, which corresponds to a gradual enhancement in consumption rate of CO_2.

This increase in CO_2 consumption rate at high current densities can be ascribed to enhanced CO_2 reduction rate and local pH effect. Higher current densities correspond to an increased conversion rate of CO_2 into gaseous and liquid products, which results in the

increment in consumption of CO_2, partially contributing to the variation of outlet flow. In addition, there is an enhanced OH^- generation rate at electrode/electrolyte interface upon increasing current densities via cathodic reactions (hydroxyl groups generation rate is linearly correlated with current densities based on Equation S(3-9)), which creates a high local pH near surface of catalyst, thus further favoring additional CO_2 consumption via Equation 1 or 2. The current induced pH variations (and concomitant CO_2 consumption) should be most obvious in moderate pH solutions. Thus as expected, a careful analysis of variation rate in gas outlet flow as a function of current density reveals a larger decrease in outlet gas flow rate with increasing current densities in moderate pH electrolyte (slope value in Figure S6: 1 M $KHCO_3$ > 1 M KOH > 5 M KOH). All the above findings imply that high-rate CO_2 reduction could result in a substantial CO_2 consumption, varying the outlet flowrate particularly in the case of high concentration of alkaline solutions.

It should be noted that the CO_2 consumption rate (flowrate alteration) is also linked to GDE surface area used in flow-electrolyzers and mass transport properties possibly influenced by type of GDEs, CO_2 inlet flow and catholyte flow. For simplification, all these parameters were kept constant in this study.

The Faradaic efficiencies of the gas products formed over Cu catalysts in different electrolytes were plotted at various current densities with and without considering the outlet flowrate changes (Figure 2). As noted in Figure 1, the gaseous product distribution is primarily ethylene across all tested current densities, with small amounts of H_2 and CO and only trace amounts of CH_4. If one would not have considered CO_2 consumption (i.e. columns with dashed line in Figure 2), it seems as if the Faradaic efficiency for C_2H_4 had a slight improvement from 1M $KHCO_3$ to 1M KOH, and then significantly increased for 5M KOH. However, there appears to be no significant variation in ethylene across all different electrolytes and current densities ranges after considering CO_2 consumption and concomitant change in outlet flow (i.e. solid columns). In addition, Hori *et al.* has demonstrated that formation of C_2 products (C_2H_4 and ethanol) are irrespective of the pH of electrolyte, but are correlated with electrode potential.[40] Here, we also found that the role of bulk pH may be minimal in affecting ethylene selectivity for CO_2 reduction at high current densities under consideration of outlet flow variation (at roughly identical potentials ranges, as shown in Table 1 and 2). Thus, the error introduced by disregarding CO_2 consumption could lead to the misunderstanding of trend in catalytic activity and erroneous conclusions about superior operating conditions.

The discrepancy in the Faradaic efficiency for C_2H_4 (major gas product) with and without considering CO_2 consumption became larger at higher current densities for the same electrolyte, as shown in Figure 2d. Notably, an overestimated Faradaic efficiency of 12% for C_2H_4 formation was discovered in 5 M KOH without considering the CO_2 consumption at 300 mA/cm^2, which is much higher compared to those in 1 M KOH (7%) and 1 M $KHCO_3$ (5.9%) under identical conditions (Figure 2d). This result indicates that Faradaic efficiencies for major gas products in flow electrolyzers at the high-rate CO_2 reduction could be significantly overestimated without

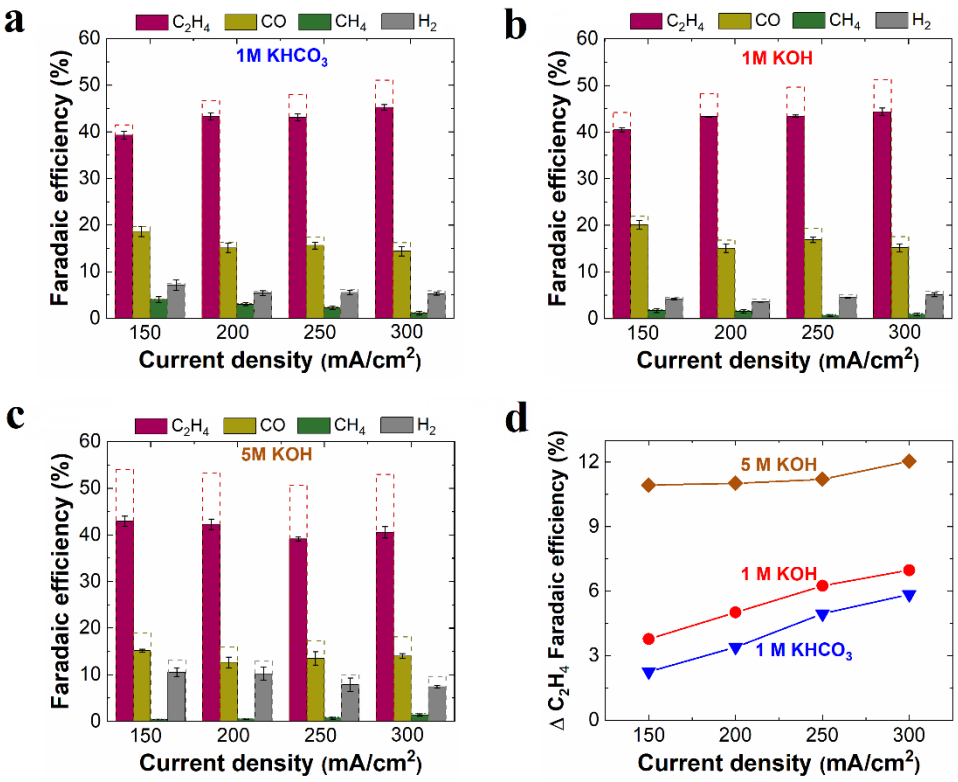

Figure 2. Comparison of the electrocatalytic performance of Cu-coated on GDEs in different electrolyte. Faradaic efficiency for gas products in 1 M $KHCO_3$ (a), 1 M KOH (b) and 5 M KOH (c) at various current densities, based on corrected and uncorrected gas flowrate, respectively (columns with dash line shows the Faradaic efficiency calculated using uncorrected gas flowrate without considering CO_2 consumption). (d) Difference in C_2H_4 Faradaic efficiency with and without the consideration of CO_2 consumption.

consideration of the CO_2 consumption (using uncorrected gas flowrate), especially for high concentration of OH^- electrolyte.

In addition to gaseous products, ethanol was observed as a major liquid product across all current densities in 1 M $KHCO_3$ and 1 M KOH, along with small amounts of n-propanol, formate and acetate as well as only trace amounts of allyl alcohol, acetaldehyde, glycolaldehyde and ethylene glycol (Figure 3). Of particular note, the selectivity of liquid products were obtained based on analysis of both catholyte and anolyte because of the fact that we found crossover of some liquid products from catholyte to anolyte via AEM (Figure S16). Specifically, while the crossover ratio of most of neutral products such as ethanol and n-propanol were very small (almost negligible), the anionic CO_2 reduction products such formate and acetate experienced substantial crossover by electromigration across all current densities (Figure S17), which is consistent with a previous report.[41] In addition, a disproportionate amount of acetaldehyde crossed to the anolyte (it appears as if the crossover ratio of acetaldehyde was relatively high) and near 20% ethanol FE (dominant liquid product in Figure 3) entail that while CO_2 reduction produced a significantly higher amount of acetaldehyde at the cathode in comparison with the detected results (Figure 3) after finishing electrolysis, most of acetaldehyde was further reduced to ethanol as the catholyte is recycled during electrolysis.[42]

Captured CO_2 throughout the electrolyte

Based on the results of Figure 1, high-rate CO_2 reduction could lead to a substantial CO_2 consumption, thus it is pertinent to understand where all CO_2 goes to achieve a complete carbon balance. With near 100% Faradaic efficiency toward all different products, the total carbon in the form of all products generation is significantly less than that of total CO_2 consumption during CO_2 reduction electrolysis. In addition to CO_2 that was converted into products, electrolyte is capable of capturing CO_2 as CO_3^{2-} or HCO_3^- (Equation 1 or 2) at electrode/electrolyte interface. In the case of 1M $KHCO_3$ as an electrolyte, substantial additional carbonate or bicarbonate formed via capturing CO_2 could not exist in electrolyte, thus there must be CO_2 degassing through either the catholyte or anolyte. A test was done in a closed-cycle catholyte with a vent for gases, a volumetric flow meter showed no gas evolution during the course of CO_2 reduction at 200 mA/cm^2. In contrast, we detected CO_2 evolution released from anolyte, accompanying with O_2 evolution (using a setup shown in Figure S8.)

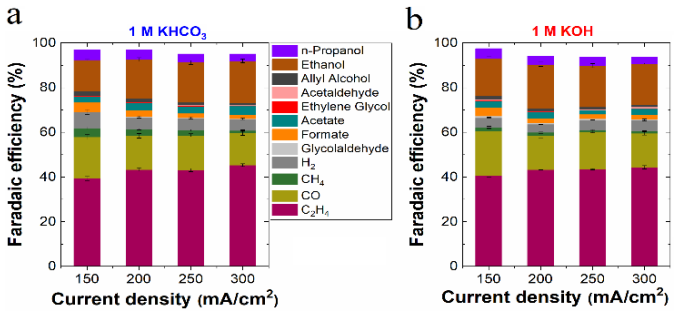

Figure 3. Faradaic efficiencies for all detected gas and liquid products in 1 M $KHCO_3$ (a) and 1 M KOH (b) at various current densities.

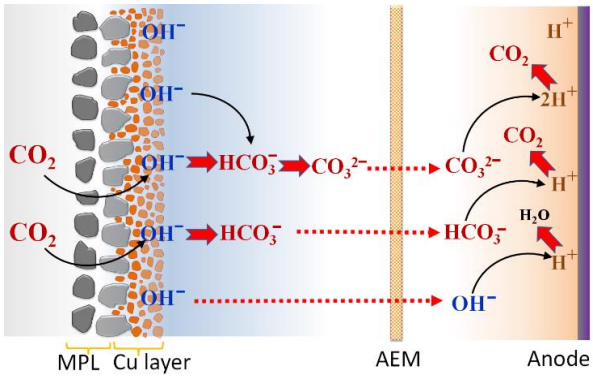

Scheme 1. (a) Proposed carbon balance paths via CO_3^{2-} or HCO_3^- formation from CO_2 and a subsequent CO_2 production from CO_3^{2-} or function of current density at steady state. 1 M $KHCO_3$ CO_3^- (red dash lines with arrows show the possible charge-carrying ionic species for AEM while using $KHCO_3$ electrolyte) in flow electrolyzers was used in all these experiments as initial catholyte (50 ml) and anolyte (50 ml).

For gaining insights into the captured CO_2 throughout the electrolyte and the released CO_2 from anolyte, Scheme 1 shows a carbon balance path through a two-step procedure of CO_3^{2-} or HCO_3^- formation from capturing CO_2 at cathode/electrolyte interface and a subsequent CO_2 generation from CO_3^{2-} or HCO_3^- at anode/electrolyte interface. In the cathodic reactions at high J ($KHCO_3$ electrolyte), a large amount of OH^- generated near the catalyst surface will react with CO_2 to form CO_3^{2-} or HCO_3^- (Equation 1 or 2), and then the anions including CO_3^{2-}, HCO_3^- or residual OH^- could transport from catholyte to anolyte via AEM as charge-carriers. Meanwhile, the pH drops locally at the anode/anolyte interface due to H^+ generation by the below anodic reaction (water oxidation reaction):

$$2H_2O \rightarrow O_2 + 4H^+ + 4e^- \quad (3)$$

Subsequently, CO_3^{2-}, HCO_3^- or OH^- coming from catholyte can neutralize the H^+ (Scheme 1) generated near the anode surface owing to the following reactions[43]:

$$HCO_3^- + H^+ \rightarrow CO_2 + H_2O \quad (4)$$

$$CO_3^{2-} + 2H^+ \rightarrow CO_2 + H_2O \quad (5)$$

$$OH^- + H^+ \rightarrow H_2O \quad (6)$$

Thus, a low local pH could lead to CO_2 degassing in anolyte which derives from the captured CO_2 by the reaction with OH^- in catholyte. After combing Equation 3 with the neutralization reactions (Equation 4-6), we can get:

$$4HCO_3^- \rightarrow 4CO_2 + O_2 + 2H_2O + 4e^- \quad (7)$$

$$2CO_3^{2-} \rightarrow 2CO_2 + O_2 + 4e^- \quad (8)$$

$$4OH^- \rightarrow 2H_2O + O_2 + 4e^- \quad (9)$$

From these simple modifications, it can be seen that the gas composition ratio of CO_2 to O_2 in anolyte will be 4, 2 and 0 if the only charge-carrier for AEM is HCO_3^-, CO_3^{2-} or OH^-, respectively. Evidently, the main charge–carrying anion species through the AEM is not only linked to CO_2 generation rate, but also can be used as an indicator of the main existing anions in catholyte. In addition, the conductivity of the membrane is also a function of ionic species.[44,45] Thus, it is highly crucial to identify whether HCO_3^-, CO_3^{2-} or potentially even OH^- is the dominant ion transferring across the AEM.

As presented in Figure 4a, the composition ratio of CO_2/O_2 gradually decreased from ~3 to ~2 in the initial 4 h, and was then maintained at ~2 for the duration of electrolysis at 200 mA/cm^2 in 1 M $KHCO_3$, implying that the main transport charge-carrier for AEM quickly changed from a mixture of HCO_3^- and CO_3^{2-} to CO_3^{2-} over electrolysis, which is attributed to the rapid transformation of HCO_3^- to CO_3^{2-} in catholyte. By combing flow meter with GC (Figure S8), a declined flowrate of CO_2 from ~5 mL/min to ~3 mL/min was observed, along with a constant O_2 flowrate over electrolysis, which is consistent with the theoretical calculation of flowrates based on that CO_3^{2-} served as the main transport charge-carriers for AEM (Figure S12).

In addition, pH of electrolyte was also measured over the course of electrolysis. Figure 4b shows that anolyte reduced to pH ~7.9 within 10 min and then maintained at natural pH throughout the rest of electrolysis, thus allowing for releasing CO_2 in anolyte. In contrast, a sharply increased catholyte pH was detected in the initial electrolysis (final pH > 11), further confirming that bicarbonate catholyte rapidly transformed to carbonate catholyte (pH of 1 M K_2CO_3 > 11).

Furthermore, analysis of gas released from anolyte was also performed at 150, 250 and 300 mA/cm^2 (Figure S9). After the system approximately reached steady state during 10 h electrolysis, the ratio of CO_2/O_2 and the corresponding flowrates of CO_2 and O_2 in Figure 4c, suggesting that CO_3^{2-} was the main transport charge-carriers which is independent of current (≥ 150 mA/cm^2) in this study. However, the catholyte transition rate from bicarbonate to carbonate was faster at higher current densities (Figure S10), due to current-dependent OH^- generation rate via cathodic reactions.

When 1 M KOH was used as an electrolyte in both anolyte (20 ml) and catholyte (20 ml), analysis of the gas from the anolyte over time (Figure 5) shows that no CO_2 was detected during the initial 2.5 h, which is due to remaining KOH in anolyte which could not allow CO_2 to exist. After 2.5 h, CO_2 started to evolve and then rapidly reached a CO_2/O_2 ratio of 2. In addition, after 5 h we found the pH of catholyte and anolyte was reduced from 13.6 to ~11.6 and ~8, respectively. These observations indicates that the CO_2 absorption in KOH at the catholyte to form carbonate, which then transferred to anolyte through the AEM. After existing KOH in anolyte was neutralized by H^+ produced in anodic reaction (Equation 3) to reach near neutral solution, CO_2 could be released via reaction of carbonate with H^+

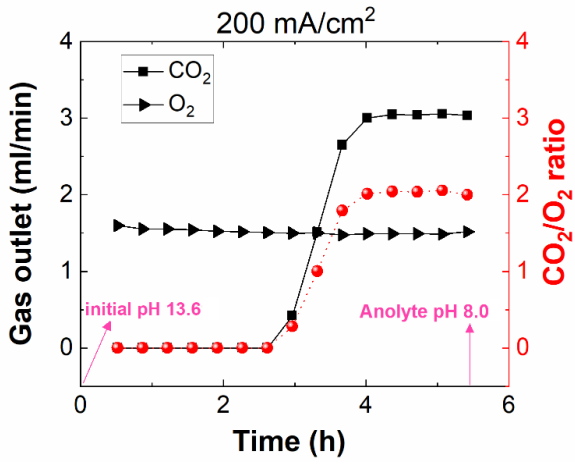

Figure 5. The flowrate of O_2 and CO_2 released from anolyte and the related CO_2/O_2 ratio over CO_2 reduction electrolysis in 1 M KOH at 200 mA/cm^2 (each bottle was filled with 20 ml of 1 M KOH as initial catholyte and anolyte).

(Scheme 1). In addition, a part of carrier ions via AEM should be carbonate (the rest is OH^-) in basic solutions in the initial 2.5 h, which leads to a large amount of existing CO_3^{2-} in anolyte before releasing CO_2 (CO_2 cannot exist in basic anolyte), thus quickly reaching a CO_2/O_2 ratio of 2 once having a neutral anolyte. It should be noted that by increasing the anolyte and catholyte volume to 50 mL, no CO_2 evolution was detected during a 6 hour test (Figure S11). These experiments demonstrate the large capacity of KOH to capture CO_2 and reiterates the point that it is essential to understand the complete carbon balance to accurately analyze CO_2 reduction.

Based on the aforementioned discussion, eventually the carbon from CO_2 inlet flow should be balanced with carbonate formation, product generation and outgoing CO_2. In the case of 1 M $KHCO_3$ as an electrolyte, the final carbon balance (Equation S14) in Figure 6a shows that the unreacted CO_2 flowrate (residual CO_2) after reactor, consumed CO_2 flowrate for carbonate formation (reaction with OH^-) and consumed CO_2 flowrate for the CO_2 conversation into products added up to a total of ~45 ml/min at various current densities, which is equal to CO_2 inlet flowrate used in this study. In addition, the total CO_2 consumption rate (carbonate formation and product generation)

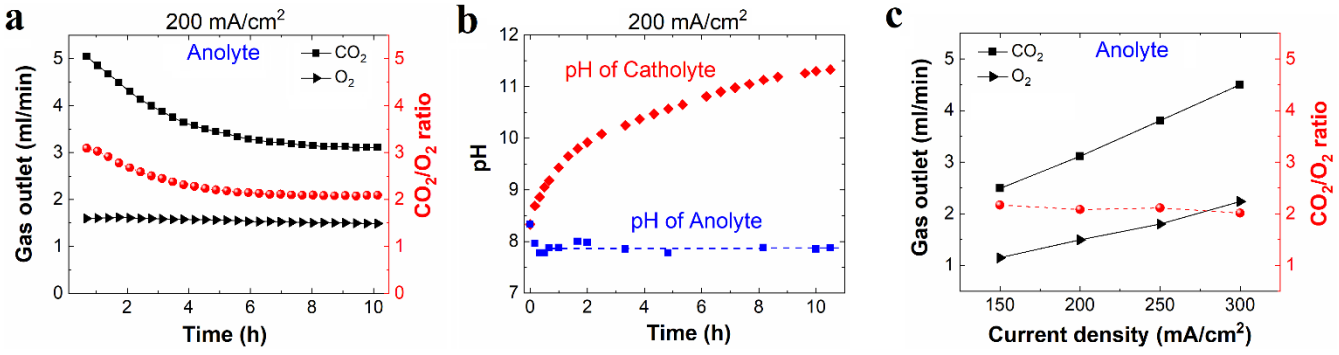

Figure 4. (a) Flowrate of CO_2 and O_2 released from anolyte, and related CO_2/O_2 ratio over time at 200 mA/cm^2. (b) Electrolyte pH over CO_2 electrolysis. (c) Flowrate of CO_2 and O_2 from anolyte as a function of current density at steady state. 1 M $KHCO_3$ was used in all these experiments as initial catholyte (50 ml) and anolyte (50 ml).

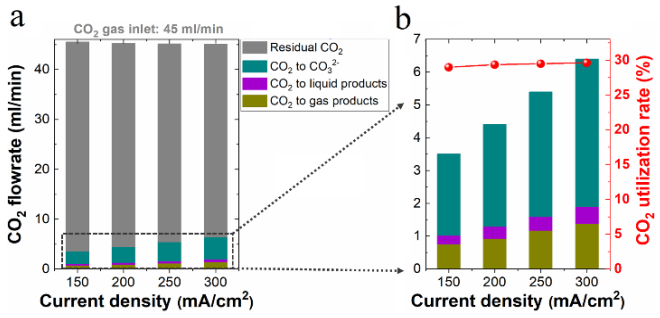

Figure 6. (a) Carbon balance for CO_2 reduction in 1 M $KHCO_3$. The total consumed CO_2 flow for carbonate formation and CO_2 reduction to all liquid and gas products as well as residual (i.e. unused) CO_2 flow were considered. (b) Ratio of CO_2 used in products formation to total CO_2 consumption (right axis).

increased as current densities enhanced (Figure 6a), which is consistent with the lower outlet flowrate for the cathode gas at higher current densities observed in Figure 1b. Notably, only ~30% of the CO_2 consumption was involved in CO_2 reduction for product formation, whereas most of consumed CO_2 (70%) was captured by the electrolyte to form carbonate (Figure 6b). Obviously, consumed CO_2 by absorbing in KOH electrolyte to carbonate formation should be much higher than that in $KHCO_3$. The fact that KOH acts as a reservoir for absorbing CO_2 complicates this analysis and greatly dilute the precision of any results while providing minimal new scientific information, thus a similar analysis for KOH solution was not done.

Conclusions

In conclusion, our results show that the CO_2 consumption via the reaction with OH^- in flow electrolyzers could significantly reduce the flowrate of gas outlet, which is closely linked to the final evaluation of the catalytic selectivity for gas products. We found the discrepancy of 5.9%, 7% and 12% for C_2H_4 FE with and without corrected flowrate at 300 mA/cm^2 in 1 M $KHCO_3$, 1 M KOH and 5 M KOH, respectively. According to the carbon balance path, the gases released from anolyte was examined during CO_2 reduction, suggesting a rapid transformation of electrolyte, which is consistent with the variation of electrolyte pH. We found that most of consumed CO_2 (~70%) at high current density CO_2 reduction in the case of 1 M $KHCO_3$ was absorbed by the electrolyte to form carbonate. In addition, 8 different liquid products were detected, accompanying with a significant amount of formate and acetate crossover through anion exchange membrane. This study presents that CO_2 consumption should be taken into account for evaluating catalytic selectivity of gas products, and both catholyte and anolyte should be analyzed for liquid products, thus enabling us to obtain reliable results for high-rate CO_2 reduction.

Conflicts of interest

There are no conflicts to declare.

Acknowledgements

This work was supported by the Villum Foundation V-SUSTAIN grant 9455 to the Villum Center for the Science of Sustainable Fuels and Chemicals. This work was also supported by ECOEthylene project from the Innovation Fund Denmark (Grant# 8057-00018B)

Notes and references

(1) Whipple, D. T.; Kenis, P. J. a. Prospects of CO2 Utilization via Direct Heterogeneous Electrochemical Reduction. *Journal of Physical Chemistry Letters* **2010**, *1* (24), 3451–3458. https://doi.org/10.1021/jz1012627.

(2) Seh, Z. W.; Kibsgaard, J.; Dickens, C. F.; Chorkendorff, I.; Nørskov, J. K.; Jaramillo, T. F. Combining Theory and Experiment in Electrocatalysis: Insights into Materials Design. *Science* **2017**, *355* (6321), eaad4998. https://doi.org/10.1126/science.aad4998.

(3) Li, C. W.; Ciston, J.; Kanan, M. W. Electroreduction of Carbon Monoxide to Liquid Fuel on Oxide-Derived Nanocrystalline Copper. *Nature* **2014**, *508* (7497), 504–507. https://doi.org/10.1038/nature13249.

(4) Qiao, J.; Liu, Y.; Hong, F.; Zhang, J. A Review of Catalysts for the Electroreduction of Carbon Dioxide to Produce Low-Carbon Fuels. *Chemical Society reviews* **2014**, *43* (2), 631–675. https://doi.org/10.1039/c3cs60323g.

(5) Ma, M.; Djanashvili, K.; Smith, W. A. Controllable Hydrocarbon Formation from the Electrochemical Reduction of CO 2 over Cu Nanowire Arrays. *Angewandte Chemie International Edition* **2016**, *55* (23), 6680–6684. https://doi.org/10.1002/anie.201601282.

(6) Zhu, D. D.; Liu, J. L.; Qiao, S. Z. Recent Advances in Inorganic Heterogeneous Electrocatalysts for Reduction of Carbon Dioxide. *Advanced Materials* **2016**, *28* (18), 3423–3452. https://doi.org/10.1002/adma.201504766.

(7) Kibria, M. G.; Edwards, J. P.; Gabardo, C. M.; Dinh, C.; Seifitokaldani, A.; Sinton, D.; Sargent, E. H. Electrochemical CO 2 Reduction into Chemical Feedstocks: From Mechanistic Electrocatalysis Models to System Design. *Advanced Materials* **2019**, *1807166*, 1807166. https://doi.org/10.1002/adma.201807166.

(8) Jiang, K.; Sandberg, R. B.; Akey, A. J.; Liu, X.; Bell, D. C.; Nørskov, J. K.; Chan, K.; Wang, H. Coupling in Electrochemical CO 2 Reduction. **2018**. https://doi.org/10.1038/s41929-017-0009-x.

(9) Chen, Y.; Li, C. W.; Kanan, M. W. Aqueous CO 2 Reduction at Very Low Overpotential on Oxide-Derived Au Nanoparticles. *Journal of the American Chemical Society* **2012**, *134* (49), 19969–19972. https://doi.org/10.1021/ja309317u.

(10) Kuhl, K. P.; Cave, E. R.; Abram, D. N.; Jaramillo, T. F. New Insights into the Electrochemical Reduction of Carbon Dioxide on Metallic Copper Surfaces. *Energy & Environmental Science*. 2012, pp 7050–7059. https://doi.org/10.1039/c2ee21234j.

(11) Kas, R.; Hummadi, K. K.; Kortlever, R.; de Wit, P.; Milbrat, A.; Luiten-Olieman, M. W. J.; Benes, N. E.; Koper, M. T. M.; Mul, G. Three-Dimensional Porous Hollow Fibre Copper Electrodes for Efficient and High-Rate Electrochemical Carbon Dioxide Reduction. *Nature Communications* **2016**, *7*, 10748. https://doi.org/10.1038/ncomms10748.

(12) Kornienko, N.; Zhao, Y.; Kley, C. S.; Zhu, C.; Kim, D.; Lin, S.; Chang, C. J.; Yaghi, O. M.; Yang, P. Metal–Organic Frameworks for Electrocatalytic Reduction of Carbon Dioxide. *Journal of the American Chemical Society* **2015**, *137* (44), 14129–14135. https://doi.org/10.1021/jacs.5b08212.

(13) Liu, M.; Pang, Y.; Zhang, B.; De Luna, P.; Voznyy, O.; Xu, J.; Zheng, X.; Dinh, C. T.; Fan, F.; Cao, C.; et al. Enhanced Electrocatalytic CO2 Reduction via Field-Induced Reagent Concentration. *Nature* **2016**, *537* (7620), 382–386. https://doi.org/10.1038/nature19060.

(14) Ma, M.; Liu, K.; Shen, J.; Kas, R.; Smith, W. A. In Situ Fabrication and Reactivation of Highly Selective and Stable Ag Catalysts for

Electrochemical CO 2 Conversion. *ACS Energy Letters* **2018**, *3* (6), 1301–1306. https://doi.org/10.1021/acsenergylett.8b00472.

(15) Ma, M.; Hansen, H. A.; Valenti, M.; Wang, Z.; Cao, A.; Dong, M.; Smith, W. A. Electrochemical Reduction of CO 2 on Compositionally Variant Au-Pt Bimetallic Thin Films. *Nano Energy* **2017**, *42* (May), 51–57. https://doi.org/10.1016/j.nanoen.2017.09.043.

(16) Hori, Y.; Takahashi, I.; Koga, O.; Hoshi, N. Selective Formation of C2 Compounds from Electrochemical Reduction of CO 2 at a Series of Copper Single Crystal Electrodes. *The Journal of Physical Chemistry B* **2002**, *106* (1), 15–17. https://doi.org/10.1021/jp013478d.

(17) Schouten, K. J. P.; Qin, Z.; Pérez Gallent, E.; Koper, M. T. M. Two Pathways for the Formation of Ethylene in CO Reduction on Single-Crystal Copper Electrodes. *Journal of the American Chemical Society* **2012**, *134* (24), 9864–9867. https://doi.org/10.1021/ja302668n.

(18) Mistry, H.; Varela, A. S.; Bonifacio, C. S.; Zegkinoglou, I.; Sinev, I.; Choi, Y.-W.; Kisslinger, K.; Stach, E. A.; Yang, J. C.; Strasser, P.; et al. Highly Selective Plasma-Activated Copper Catalysts for Carbon Dioxide Reduction to Ethylene. *Nature Communications* **2016**, *7* (1), 12123. https://doi.org/10.1038/ncomms12123.

(19) Burdyny, T.; Smith, W. A. CO 2 Reduction on Gas-Diffusion Electrodes and Why Catalytic Performance Must Be Assessed at Commercially-Relevant Conditions. *Energy & Environmental Science* **2019**, *12* (5), 1442–1453. https://doi.org/10.1039/C8EE03134G.

(20) Weng, L. C.; Bell, A. T.; Weber, A. Z. Modeling Gas-Diffusion Electrodes for CO2 Reduction. *Physical Chemistry Chemical Physics* **2018**, *20* (25), 16973–16984. https://doi.org/10.1039/c8cp01319e.

(21) Dinh, C.-T.; Burdyny, T.; Kibria, M. G.; Seifitokaldani, A.; Gabardo, C. M.; García de Arquer, F. P.; Kiani, A.; Edwards, J. P.; De Luna, P.; Bushuyev, O. S.; et al. CO 2 Electroreduction to Ethylene via Hydroxide-Mediated Copper Catalysis at an Abrupt Interface. *Science* **2018**, *360* (6390), 783–787. https://doi.org/10.1126/science.aas9100.

(22) Möller, T.; Ju, W.; Bagger, A.; Wang, X.; Luo, F.; Ngo Thanh, T.; Varela, A. S.; Rossmeisl, J.; Strasser, P. Efficient CO 2 to CO Electrolysis on Solid Ni–N–C Catalysts at Industrial Current Densities. *Energy & Environmental Science* **2019**, *12* (2), 640–647. https://doi.org/10.1039/C8EE02662A.

(23) Kibria, M. G.; Dinh, C. T.; Seifitokaldani, A.; De Luna, P.; Burdyny, T.; Quintero-Bermudez, R.; Ross, M. B.; Bushuyev, O. S.; García de Arquer, F. P.; Yang, P.; et al. A Surface Reconstruction Route to High Productivity and Selectivity in CO 2 Electroreduction toward C 2+ Hydrocarbons. *Advanced Materials* **2018**, *30* (49), 1–7. https://doi.org/10.1002/adma.201804867.

(24) Dinh, C. T.; García De Arquer, F. P.; Sinton, D.; Sargent, E. H. High Rate, Selective, and Stable Electroreduction of CO2 to Co in Basic and Neutral Media. *ACS Energy Letters* **2018**, *3* (11), 2835–2840. https://doi.org/10.1021/acsenergylett.8b01734.

(25) Verma, S.; Lu, X.; Ma, S.; Masel, R. I.; Kenis, P. J. A. The Effect of Electrolyte Composition on the Electroreduction of CO2 to CO on Ag Based Gas Diffusion Electrodes. *Physical Chemistry Chemical Physics* **2016**, *18* (10), 7075–7084. https://doi.org/10.1039/c5cp05665a.

(26) Endrődi, B.; Bencsik, G.; Darvas, F.; Jones, R.; Rajeshwar, K.; Janáky, C. Continuous-Flow Electroreduction of Carbon Dioxide. *Progress in Energy and Combustion Science* **2017**, *62*, 133–154. https://doi.org/10.1016/j.pecs.2017.05.005.

(27) Jouny, M.; Luc, W.; Jiao, F. High-Rate Electroreduction of Carbon Monoxide to Multi-Carbon Products. *Nature Catalysis* **2018**, *1* (10), 748–755. https://doi.org/10.1038/s41929-018-0133-2.

(28) Hoang, T. T. H.; Verma, S.; Ma, S.; Fister, T. T.; Timoshenko, J.; Frenkel, A. I.; Kenis, P. J. A.; Gewirth, A. A. Nanoporous Copper–Silver Alloys by Additive-Controlled Electrodeposition for the Selective Electroreduction of CO 2 to Ethylene and Ethanol. *Journal of the American Chemical Society* **2018**, *140* (17), 5791–5797. https://doi.org/10.1021/jacs.8b01868.

(29) Kim, B.; Hillman, F.; Ariyoshi, M.; Fujikawa, S.; Kenis, P. J. A. Effects of Composition of the Micro Porous Layer and the Substrate on Performance in the Electrochemical Reduction of CO 2 to CO. *Journal of Power Sources* **2016**, *312*, 192–198. https://doi.org/10.1016/j.jpowsour.2016.02.043.

(30) Gabardo, C. M.; Seifitokaldani, A.; Edwards, J. P.; Dinh, C. T.; Burdyny, T.; Kibria, M. G.; O'Brien, C. P.; Sargent, E. H.; Sinton, D. Combined High Alkalinity and Pressurization Enable Efficient CO2 Electroreduction to CO. *Energy and Environmental Science* **2018**, *11* (9), 2531–2539. https://doi.org/10.1039/c8ee01684d.

(31) Ma, S.; Sadakiyo, M.; Heima, M.; Luo, R.; Haasch, R. T.; Gold, J. I.; Yamauchi, M.; Kenis, P. J. A. Electroreduction of Carbon Dioxide to Hydrocarbons Using Bimetallic Cu–Pd Catalysts with Different Mixing Patterns. *Journal of the American Chemical Society* **2017**, *139* (1), 47–50. https://doi.org/10.1021/jacs.6b10740.

(32) De Luna, P.; Quintero-Bermudez, R.; DInh, C. T.; Ross, M. B.; Bushuyev, O. S.; Todorović, P.; Regier, T.; Kelley, S. O.; Yang, P.; Sargent, E. H. Catalyst Electro-Redeposition Controls Morphology and Oxidation State for Selective Carbon Dioxide Reduction. *Nature Catalysis* **2018**, *1* (2), 103–110. https://doi.org/10.1038/s41929-017-0018-9.

(33) Lv, J.-J.; Jouny, M.; Luc, W.; Zhu, W.; Zhu, J.-J.; Jiao, F. A Highly Porous Copper Electrocatalyst for Carbon Dioxide Reduction. *Advanced Materials* **2018**, *30* (49), 1803111. https://doi.org/10.1002/adma.201803111.

(34) Luc, W.; Ko, B. H.; Kattel, S.; Li, S.; Su, D.; Chen, J. G.; Jiao, F. SO 2 -Induced Selectivity Change in CO 2 Electroreduction. *Journal of the American Chemical Society* **2019**, *141* (25), 9902–9909. https://doi.org/10.1021/jacs.9b03215.

(35) Verma, S.; Hamasaki, Y.; Kim, C.; Huang, W.; Lu, S.; Jhong, H.-R. M.; Gewirth, A. A.; Fujigaya, T.; Nakashima, N.; Kenis, P. J. A. Insights into the Low Overpotential Electroreduction of CO 2 to CO on a Supported Gold Catalyst in an Alkaline Flow Electrolyzer. *ACS Energy Letters* **2018**, *3* (1), 193–198. https://doi.org/10.1021/acsenergylett.7b01096.

(36) Wang, R.; Haspel, H.; Pustovarenko, A.; Dikhtiarenko, A.; Russkikh, A.; Shterk, G.; Osadchii, D.; Ould-Chikh, S.; Ma, M.; Smith, W. A.; et al. Maximizing Ag Utilization in High-Rate CO 2 Electrochemical Reduction with a Coordination Polymer-Mediated Gas Diffusion Electrode. *ACS Energy Letters* **2019**, *4* (8), 2024–2031. https://doi.org/10.1021/acsenergylett.9b01509.

(37) Li, Y. C.; Zhou, D.; Yan, Z.; Gonçalves, R. H.; Salvatore, D. A.; Berlinguette, C. P.; Mallouk, T. E. Electrolysis of CO2 to Syngas in Bipolar Membrane-Based Electrochemical Cells. *ACS Energy Letters* **2016**, *1* (6), 1149–1153. https://doi.org/10.1021/acsenergylett.6b00475.

(38) Larrazábal, G. O.; Strøm-Hansen, P.; Heli, J. P.; Zeiter, K.; Therkildsen, K. T.; Chorkendorff, I.; Seger, B. Analysis of Mass Flows and Membrane Crossover in CO2 Reduction at High Current Densities in a MEA-Type Electrolyzer. *ACS Applied Materials & Interfaces* **2019**, acsami.9b13081. https://doi.org/10.1021/acsami.9b13081.

(39) Lebedev, Y. A.; Korolev, Y. M.; Polikarpov, V. M.; Ignat'ev, L. N.; Antipov, E. M. X-Ray Powder Diffraction Study of Polytetrafluoroethylene. *Crystallography Reports* **2010**, *55* (4), 609–614. https://doi.org/10.1134/S1063774510040127.

(40) Hori, Y.; Takahashi, R.; Yoshinami, Y.; Murata, A. Electrochemical Reduction of CO at a Copper Electrode. *The Journal of Physical Chemistry B* **1997**, *101* (36), 7075–7081. https://doi.org/10.1021/jp970284i.

(41) Li, Y. C.; Yan, Z.; Hitt, J.; Wycisk, R.; Pintauro, P. N.; Mallouk, T. E. Bipolar Membranes Inhibit Product Crossover in CO 2 Electrolysis Cells. *Advanced Sustainable Systems* **2018**, *2* (4), 1700187. https://doi.org/10.1002/adsu.201700187.

(42) Clark, E. L.; Bell, A. T. Direct Observation of the Local Reaction Environment during the Electrochemical Reduction of CO 2. *Journal of the American Chemical Society* **2018**, *140* (22), 7012–7020. https://doi.org/10.1021/jacs.8b04058.

(43) Zhong, H.; Fujii, K.; Nakano, Y.; Jin, F. Effect of CO2 Bubbling into Aqueous Solutions Used for Electrochemical Reduction of CO2 for Energy Conversion and Storage. *Journal of Physical Chemistry C* **2015**, *119* (1), 55–61. https://doi.org/10.1021/jp509043h.

(44) Deavin, O. I.; Murphy, S.; Ong, A. L.; Poynton, S. D.; Zeng, R.; Herman, H.; Varcoe, J. R. Anion-Exchange Membranes for Alkaline Polymer Electrolyte Fuel Cells: Comparison of Pendent Benzyltrimethylammonium- and Benzylmethylimidazolium-Head-Groups. *Energy & Environmental Science* **2012**, *5* (9), 8584. https://doi.org/10.1039/c2ee22466f.

(45) Varcoe, J. R.; Atanassov, P.; Dekel, D. R.; Herring, A. M.; Hickner, M. A.; Kohl, P. A.; Kucernak, A. R.; Mustain, W. E.; Nijmeijer, K.; Scott, K.; et al. Anion-Exchange Membranes in Electrochemical Energy Systems. *Energy Environ. Sci.* **2014**, *7* (10), 3135–3191. https://doi.org/10.1039/C4EE01303D.

Supporting Information

Insights into the Carbon Balance for CO2 Electroreduction on Cu using Gas Diffusion Electrode Reactor Designs

Ming Ma,[†] Ezra L. Clark,[†] Kasper T. Therkildsen,[‡] Sebastian Dalsgaard,[†] Ib Chorkendorff[†] and Brian Seger[†,*]

[†]Department of Physics, Technical University of Denmark, 2800 Kgs Lyngby, Denmark

[‡]Siemens A/S, RC-DK SI, Diplomvej 378, 2800 Kgs. Lyngby, Denmark

*Author to whom correspondence should be addressed.

E-mail address: brse@fysik.dtu.dk

Tel.: +45 45253174

Materials

Potassium bicarbonate ($KHCO_3$, ≥99.95%) and potassium hydroxide hydrate ($NaOH \cdot xH_2O$, 99.995%, Suprapur®) were purchased from Sigma Aldrich. All chemicals were used in this study without further purification. Anion exchange membrane (AEM, Fumasep FAA-3-PK-75) and gas-diffusion electrode (GDE, Sigracet 39 BC) were purchased from Fuel Cell Store. Iridium dioxide (IrO_2) purchased from Dioxide Materials was used as anode in CO_2 flow electrolyzers.

Catalysts fabrication and characterization

In this work, Cu catalsyts were deposited on the top of microporous layer of gas-diffusion electrodes by direct current magnetron sputtering from a Cu target. In order to obtain the accurate deposition rate of Cu, Cu films were deposited on Si substrates, and then the cross-sectional SEM of Cu film/Si was peformed. Figure S1 shows the cross-sectional SEM image of Cu film/Si deposited for 50 min, which indicates the fact that ~200 nm thick Cu film was synthesized, corresponding to a Cu depositon rate of ~4 nm/min.

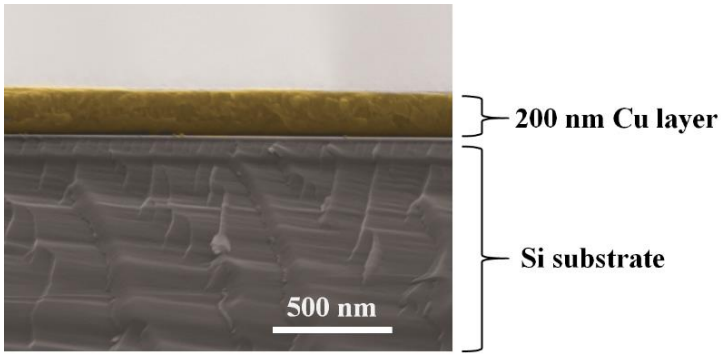

Figure S1. Cross-sectional SEM image of Cu layer deposited on Si by magnetron sputtering for 50 min.

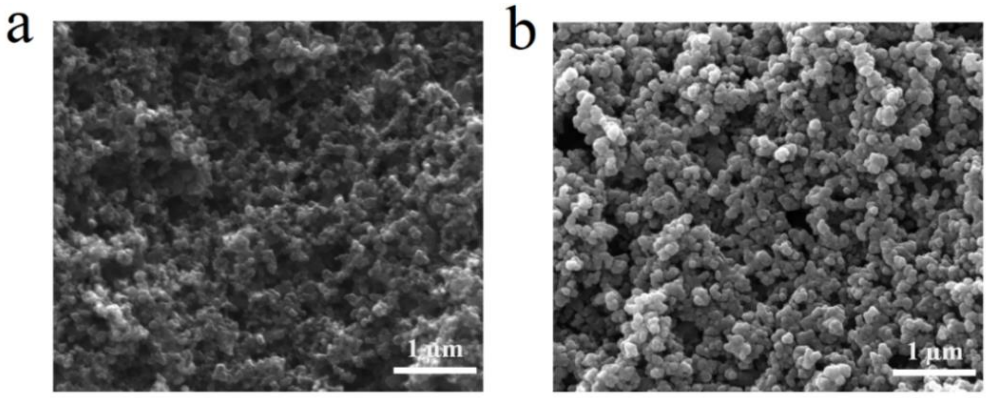

Figure S2. SEM images of microporous carbon layers (a) of gas-diffusion electrodes and Cu catalysts (b) coated on microporous carbon layers of gas-diffusion electrodes.

Figure S3. Digital image of Cu deposited on a gas-diffusion electrode.

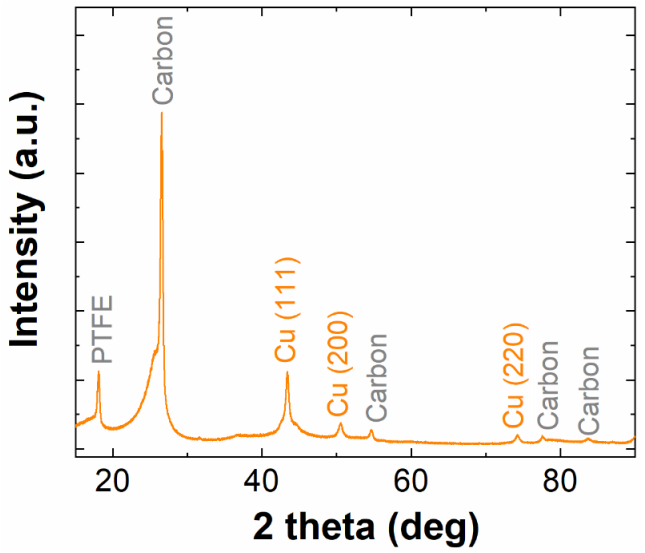

Figure S4. XRD patterns of Cu coated on a gas-diffusion electrode (Sigracet 39 BC). XRD measurements were performed using Cu Kα radiation.

Faradaic efficiency calculation

The Faradaic efficiency (FE) of products can be calculated according to the below equation:

$$FE\ (\%) = \frac{Q_{product}}{Q_{tot}} \times 100\% \qquad (S1)$$

where $Q_{product}$ and Q_{tot} are charge transferred for product formation and charge passed through the working electrode, respectively.

Based on the above equation, the detailed caculation for Faradaic efficiency of gas products could be written as:

$$FE\ (\%) = \frac{n \times C_{product} \times \emptyset t \times \frac{P_o}{RT} \times F}{I \times t} \times 100\% \qquad (S2)$$

where $C_{product}$ and n are the concentration of gas product measured by GC and the number of electrons required for producing one molecule of the related gas product, respectively. $\emptyset$ is gas flow rate, t is the electrolysis time, P_o is ambient pressure, F is Faraday constant, , R is ideal gas constant, T is absolute temperature, and I is current.

High local pH at cathode/electrolyte interface

In the electrocatalytic CO_2 reduction process, CO_2 can be converted into a variety of gas and liquid products when combined with water on metal surfaces in aqueous solutions according to the reactions[1–3]:

$$CO_2 + H_2O + 2e^- \rightarrow CO + 2OH^- \quad \text{(-0.11 V vs. RHE)} \quad \text{(S3)}$$

$$CO_2 + 6H_2O + 8e^- \rightarrow CH_4 + 8OH^- \quad \text{(0.17 V vs. RHE)} \quad \text{(S4)}$$

$$2CO_2 + 8H_2O + 12e^- \rightarrow C_2H_4 + 12OH^- \quad \text{(0.08 V vs. RHE)} \quad \text{(S5)}$$

$$CO_2 + H_2O + 2e^- \rightarrow HCOO^- + OH^- \quad \text{(-0.03 V vs. RHE)} \quad \text{(S6)}$$

$$CO_2 + 5H_2O + 6e^- \rightarrow CH_3OH + 6OH^- \quad \text{(0.03 V vs. RHE)} \quad \text{(S7)}$$

$$2CO_2 + 9H_2O + 12e^- \rightarrow C_2H_5OH + 12OH^- \quad \text{(0.09 V vs. RHE)} \quad \text{(S8)}$$

The competing H_2 evolution is an unavoidable reaction in CO_2 electroreduction. Thus, water is reduced to H_2 on the surface of catalyst according to the reaction[1]:

$$2H_2O + 2e^- \rightarrow H_2 + 2OH^- \quad \text{(0 V vs. RHE)} \quad \text{(S9)}$$

Thus, OH^- ions are produced at the cathode/electrolyte interface in the cathodic reactions (Equation (3-9)), leading to an increased pH near the surface of cathode.[2,3]

Reaction of CO_2 and OH^- near cathode surface

In addition to the electrochemcial CO_2 reduction, CO_2 also can react with OH^- created at the electrode/electrolyte interface by cathodic reactions (Equation (S3-S9)) using $KHCO_3$ electrolye in our three-compartment flow electrolyzer. Of particular note, CO_2 not only reacts with OH^- generated by cathodic reactions (Equation (S3-S9)) but also reacts with OH^- derived from electrolyte during CO_2 electroreduction in KOH solutions.

CO_2 reduction and flowrate mesurement of gas outlet after cell

The electroreduction of CO_2 was conducted in a three-compartment flow electrolyzer made from Teflon at ambient temperature and pressure. In the cell, catholyte and anolyte flow compartments are separated by an anion exchange membrane, along with continuous flow electrolyte (each bottle is filled with 50 ml electrolyte), as shown in Figure S5. In addition, CO_2 was fed into gas chamber at a constant flow rate of 45 ml/min, and then gaseous CO_2 could pass through the gas-diffusion layer, diffusing into the surface of the catalyst which was immesed into electrolyte.

During the electroreduction of CO_2, the gas mixture (gas outlet) after reactor was directly vented into the gas-sampling loop of a GC for periodic quantificaiton of gas products. In order to get the reliable Faradaic efficiency of gas prouduts, the volumetric flowrate of gas outlet (gas mixture) after reactor was also measured by flow meter during the CO_2 reduction, as displayed in Figure S5. Gas outlet flowrate from the gas chamber after CO_2 reduction was plotted at various current densities for 1 M $KHCO_3$, 1 M KOH and 5 M KOH electrolyte, respectively (Figure S6). As noted in Figure S6, an obvious decrement in the flowrate of outlet was detected with increasing current densities in the same electrolyte. Here, we calculated the decrease rate of outlet flowrate as a function of current density in 1 M $KHCO_3$, 1 M KOH and 5 M KOH electrolyte, respectively (slope values in Figure S6).

In addition, gas outlet flowrate (or CO_2 consumption) should also be correlated with the surface area of Cu coated on GDE. Thus, a fixed geometric surface area (2 cm^2) of Cu layer was utilized for all the experiments in this study.

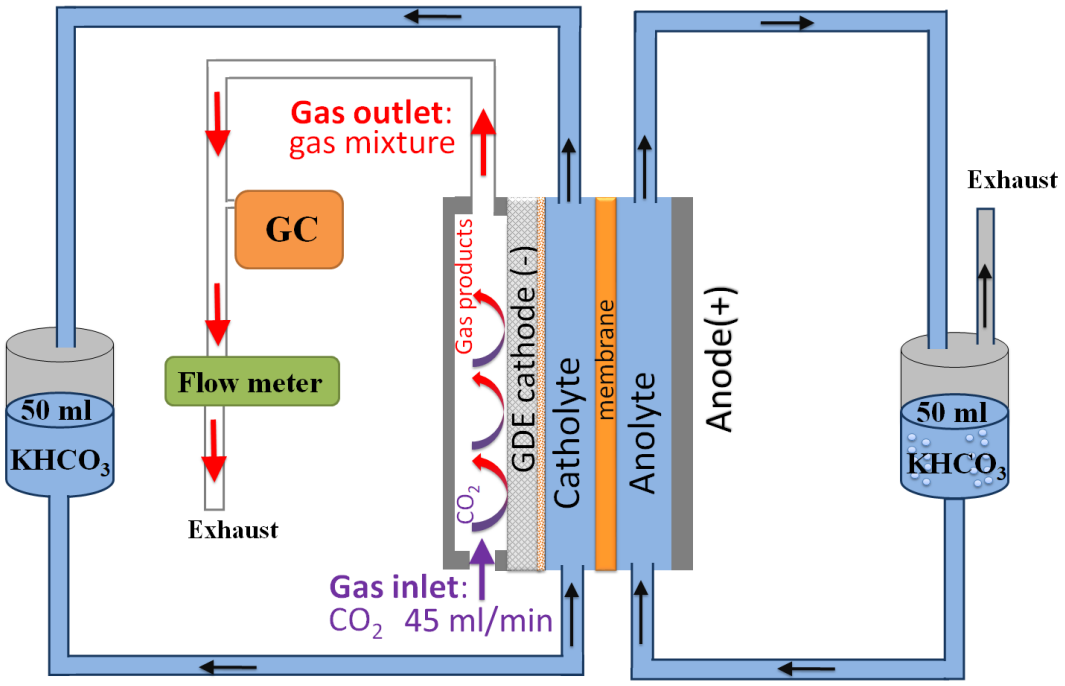

Figure S5. The schematic illustration of flow cell setup for reduction of CO_2.

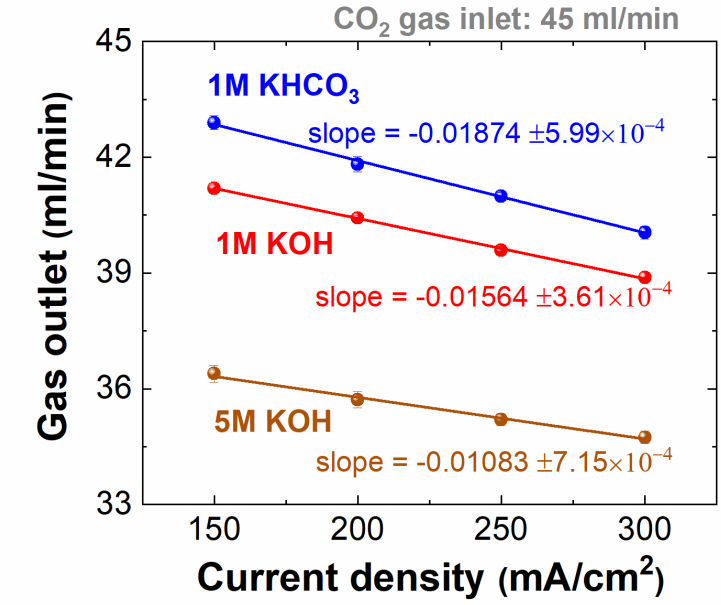

Figure S6. Gas outlet flowrates from the gas chamber after CO_2 reduction at various current densities in 1 M $KHCO_3$ (pH 8.33), 1 M KOH (pH 13.61) and 5 M KOH electrolyte, respectively (geometric surface area of Gu layer on GDE is 2 cm^2).

CO_2 reduction performance

Based on the aforementioned flowrate measurement, the volumetric flowrate of gas outlet (gas mixture) after reactor was mornitored by flow meter in the course of the CO_2 reduction, and then Faradaic efficiencies of gas products were calcuated based on the mornitored outlet flowrate. Figure S7 shows the typical catalytic selectivity of gas products over time in 1 M $KHCO_3$ (a) and 1 M KOH (b) at 200 mA/cm^2, respectivily.

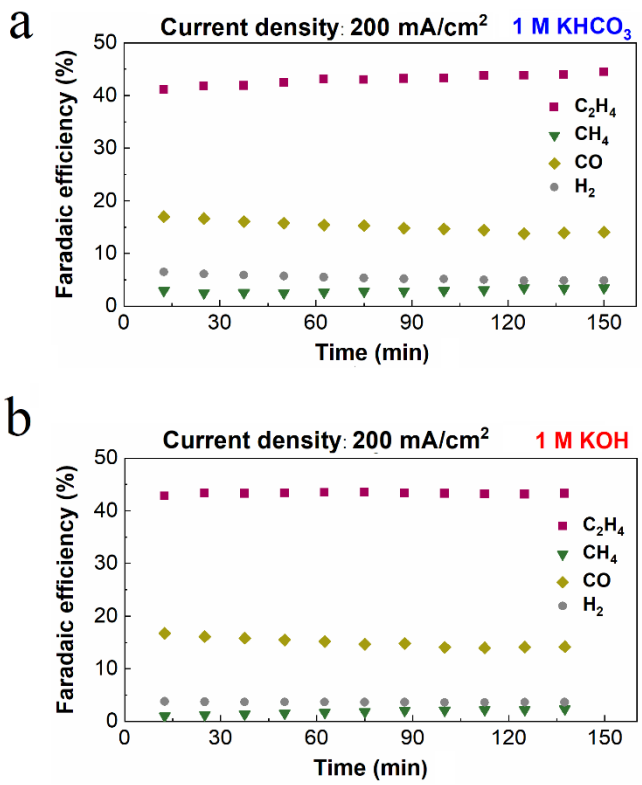

Figure S7. Catalytic selectivity of gas products over Cu catalylsts in 1 M $KHCO_3$ (a) and 1 M KOH (b) at 200 mA/cm^2, respectivily. All the tests were performed using 70 nm Cu layer coated on GDEs.

Analysis of gas released from anolyte

CO_2 reduction with the competing H_2 evolution takes place on the surface of cathode while O_2 evolution happens on the anode surface. Interestingly, H^+ created at the anode/electrolyte interface by anodic reaction (Equation 3) could be neutralized by HCO_3^- or CO_3^{2-} after using $KHCO_3$ electrolyte. According to the reactions (Equation 7-8), gaseous CO_2 should be also released from $KHCO_3$ anolyte, accompanying with O_2. The flow cell setup for reduction of CO_2 in Figure S8 was used to analyse the gases released from anolyte. Specifically, gases released from anolyte were diluted with N_2 carrier gas at a constant flowrate, and then directly went into the gas sampling-loop of the GC to quantify the gases periodically. In addition, the volumetric gas flowrate released from anolyte was also mornitored by flow meter over the CO_2 reduction electrolysis (Figure S8).

After using 1 M $KHCO_3$ as electrolyte for CO_2 reduction, CO_2 released from anolyte was detected via GC, accompanying with O_2 at various current densities (Figure S9). In addition, the related CO_2/O_2 ratio released from anolyte over CO_2 reduction electrolysis at current densities of 150 mA/cm^2, 250 mA/cm^2, 300 mA/cm^2 using 1 M $KHCO_3$ as the initial catholyte and anolyte was also presented in Figure S9.

In contrast, only O_2 (~1.5 ml/min) was detected from anolyte at 200 mA/cm^2 over 6 h electrolysis after using 1 M KOH (Figure S11), due to a slow transition of electrolyte caused by the large amount of KOH (each bottle was filled with 50 ml 1 M KOH as initial catholyte and anolyte). For observing a relatively rapid electrolyte transition, each bottle (initial catholyte and anolyte) was filled with 20 ml 1 M KOH, discovering the initial CO_2 generation from anolyte after 2.5 h electrolysis, as shown in Figure 5.

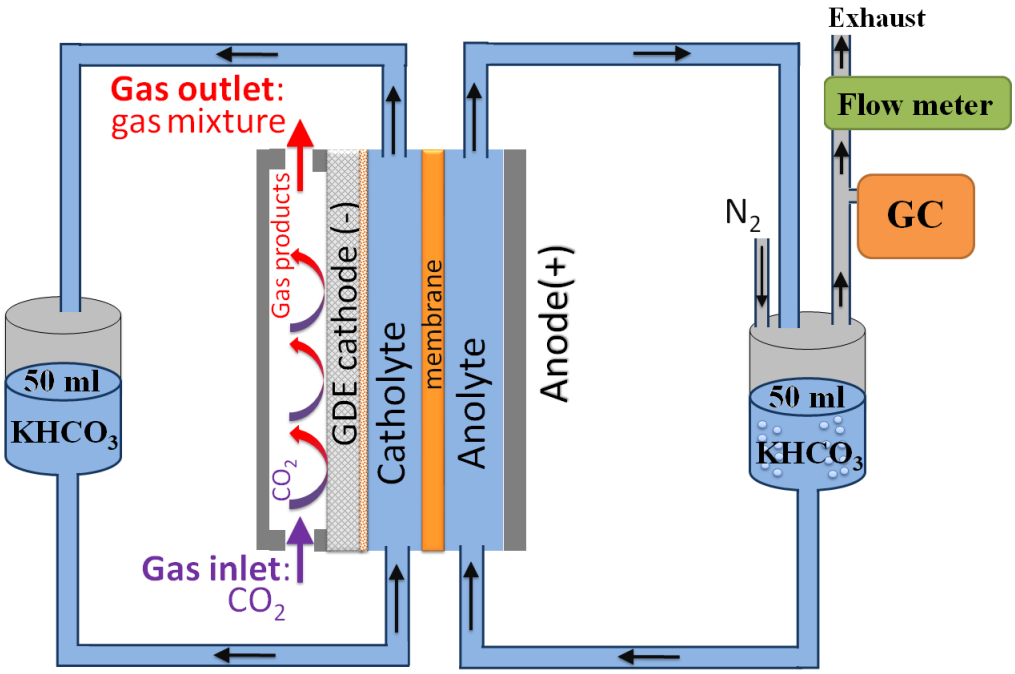

Figure S8. The schematic illustration of flow cell setup for analysing gases released from anolyte during CO_2 reduction.

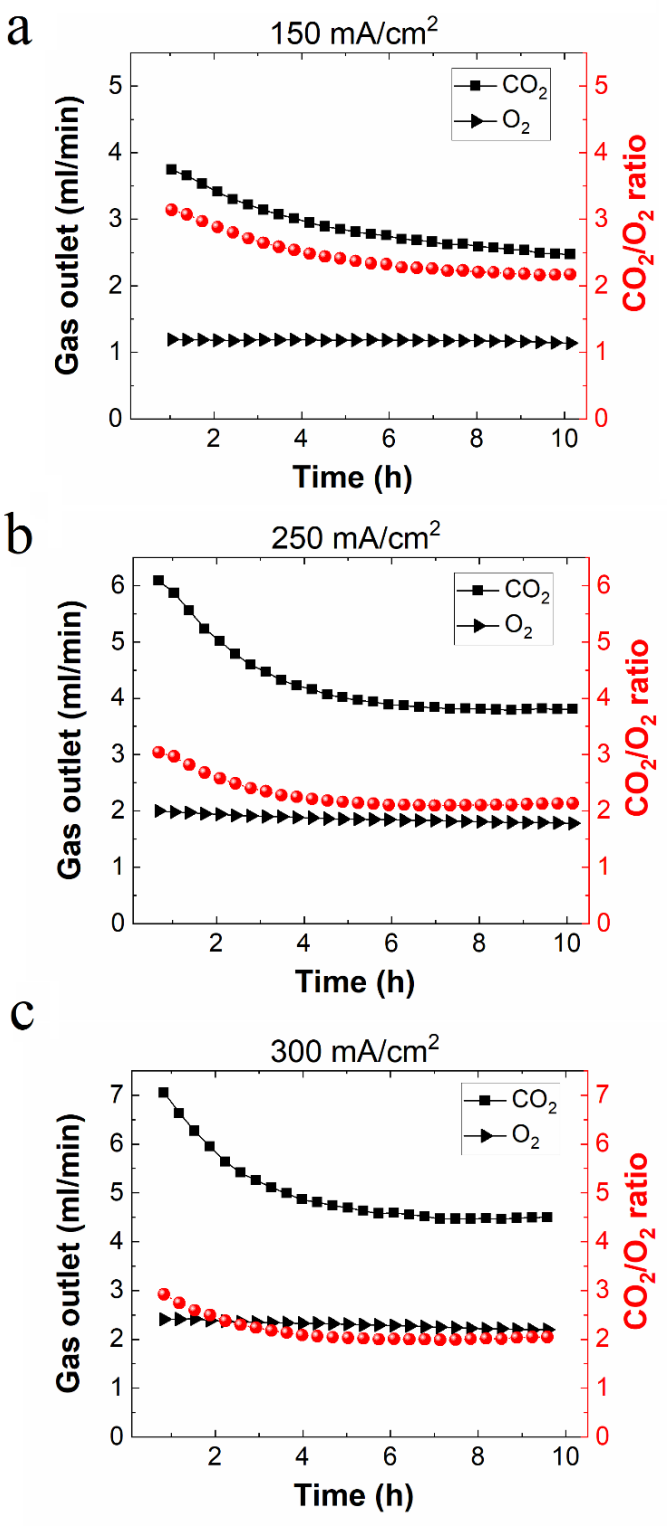

Figure S9. The flowrate of O_2 and CO_2 released from anolyte and the related CO_2/O_2 ratio over CO_2 reduction electrolysis at current densities of (a) 150 mA/cm^2, (b) 250 mA/cm^2, (c) 300 mA/cm^2 using 1 M $KHCO_3$ as the initial catholyte and anolyte (each both was filled with 50 ml 1 M $KHCO_3$ electrolyte).

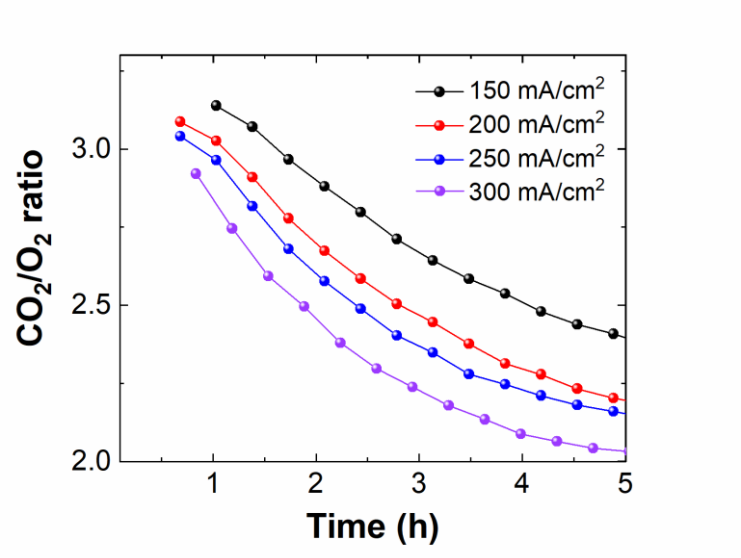

Figure S10. CO_2/O_2 flowrate ratio released from anolyte as a function of time at various current densities after using 1 M $KHCO_3$ as the initial catholyte and anolyte (each bottle was filled with 50 ml 1 M $KHCO_3$ electrolyte).

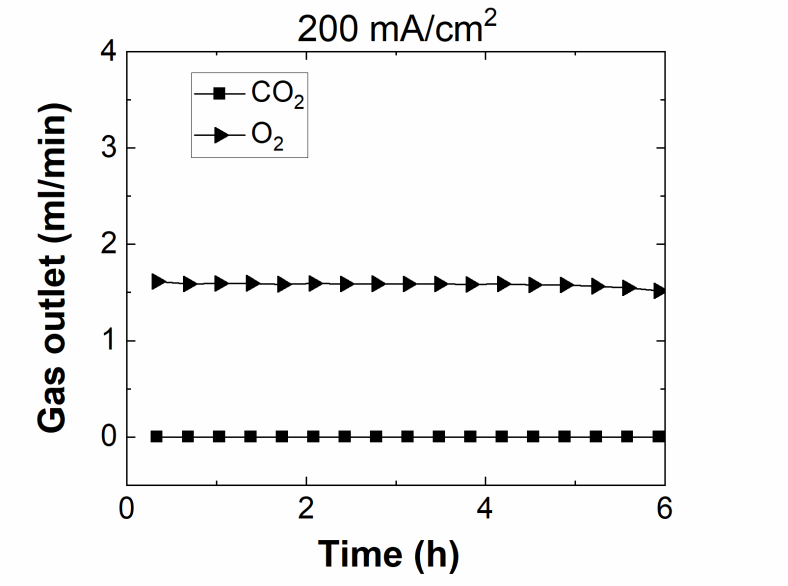

Figure S11. The flowrate of O_2 and CO_2 released from anolyte over CO_2 reduction electrolysis in 1 M KOH (each bottle was filled with 50 ml 1 M KOH as initial catholyte and anolyte).

Theoretical O_2 and CO_2 flowrate released from anolyte

If charge passed through anode is only used for O_2 evolution reaction, O_2 flowrate released in anolyte can be expressed as:

$$\emptyset\ (O_2) = \frac{Q_{tot}}{nF} \times \frac{RT}{P_o} \qquad (S10)$$

where Q_{tot} and n are charge passed through the anode electrode and the number (here is 4) of holes required for producing one O_2 molecule, respectively. *F* is Faradaic constant, *R* is ideal gas constant, T is absolute temperature, and P_o is ambient pressure.

If bicarbonate or carbonate is the only charge-carrier via anion exhange membrane (AEM), the CO_2 flowrate should be $4 \times \emptyset\ (O_2)$ and $2 \times \emptyset\ (O_2)$ according to the Equation (7) and Equation (8), respectively. Based on these equations, the flowrate for CO_2 and O_2 was calculated at various current densities (electrode surface area is 2 cm^2), as shown in Figure S12.

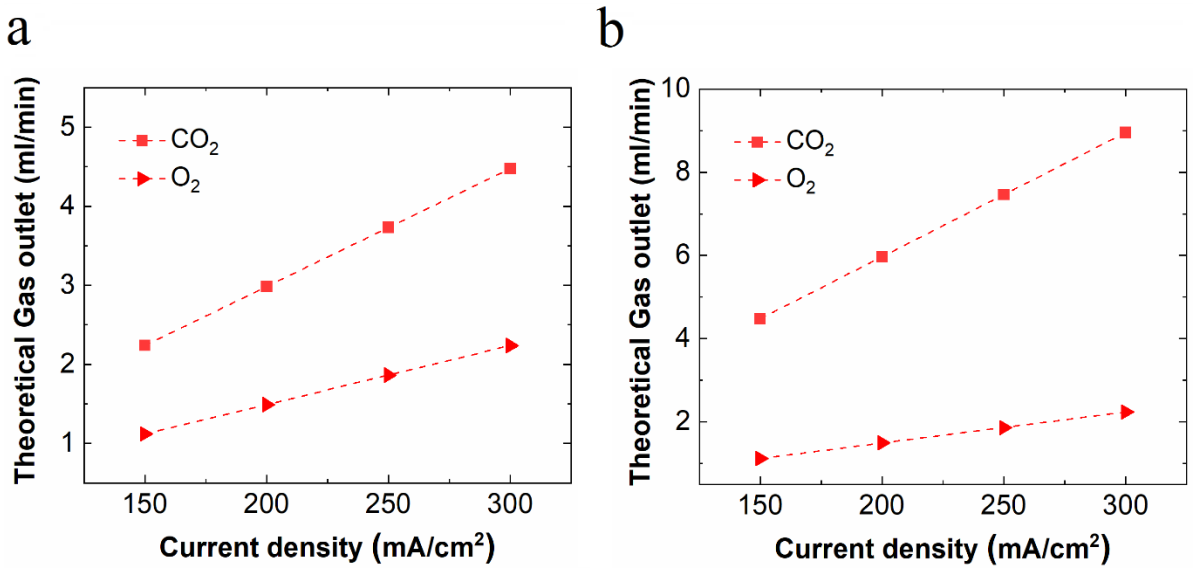

Figure S12. The estimated flowrate of O_2 and CO_2 released from anolyte as a function of current density based on the only charge-carrier via AEM is carbonate (a) and bicarbonate (b).

Carbon balance calculation

The unreacted CO_2 (residual CO_2) flowrate in the gas outlet (gas mixture) after reactor can be expressed as:

$$\emptyset_{residual\ CO_2} = \emptyset_{outlet} - (\emptyset_{CO} + \emptyset_{CH_4} + \emptyset_{C_2H_4} + \emptyset_{H_2}) \quad (S11)$$

where $\emptyset_{outlet}$ is the flowrate of gas outlet from the gas chamber after CO_2 reduction. $\emptyset_{CO}$, $\emptyset_{CH_4}$, $\emptyset_{C_2H_4}$ and $\emptyset_{H_2}$ are the gas flowrate of CO, CH_4, C_2H_4 and H_2 in the gas outlet from gas chamber during electrolysis, respectively.

The consumed CO_2 flowrate which is electrochemcially converted into all gas products (CO, C_2H_4 and CH_4) can be written as:

$$\emptyset_{CO_2\ to\ gas} = \emptyset_{CO} + \emptyset_{CH_4} + 2\emptyset_{C_2H_4} \quad (S12)$$

The consumed CO_2 flowrate for electrocatalytic reduction to all liquid products (such as ethanol and formate) can be written as:

$$\emptyset_{CO_2\ to\ liquid} = \emptyset_{C_1} + \emptyset_{C_2} + \emptyset_{C_3} \quad (S13)$$

where $\emptyset_{C_1}$, $\emptyset_{C_2}$, and $\emptyset_{C_3}$ are the consumed CO_2 flowrate for forming C_1, C_2 and C_3 liquid products, respectively.

CO_2 reduction at high reaction rates, CO_2 conversion into gas products (> C_1) and liquid products could reduce the gas outlet flowrate. In addition, the CO_2 consumption at high current via the reaction between OH^- and CO_2 could significantly contribute to the decrease of the total gas outlet flowrate (Figure S6). Thus, the carbon element from CO_2 inlet flowrate should be eventually balanced by the below equation:

$$\emptyset_{inlet\ CO_2} = \emptyset_{residual\ CO_2} + \emptyset_{CO_2\ to\ gas} + \emptyset_{CO_2\ to\ liquid} + \emptyset_{OH^-} \quad (S14)$$

where $\emptyset_{OH^-}$ is the consumed CO_2 flowrate via the reaction with OH^- (Equation 1 or 2).

Electrochemical impedance spectroscopy measurement

To determine the solution resistance (Rs) in this work, potentiostatic electrochemical impedance spectroscopy (PEIS) was performed on Cu deposited GDE in a three-compartment flow electrolyzer at room temperature and atmospheric pressure.[4] During the experiments, the gas flow compartment was continuously fed with CO_2 at a flow rate of 45 ml/min. The impedance spectra were recorded using a potentiostat (Biologic) in the frequency range from 200 kHz to 10 mHz with an amplitude of 10 mV at fixed potentials. It should be noted that the variations in local ion species and concentration near surface of cathode at high-rate cathodic reactions could make the local reaction environment complicated, and also lead to a distinct conductivity near cathode at high current densities compared to the measured results by PEIS. Even if a very tiny difference in resistance, a very high current could lead to an un-negligible variation in IR-corrected potentials. Thus, while the fixed distance between reference and cathode was less than 2 mm in this work, it is still difficult to get the accurate cathode potentials at relatively high current densities (for instance, the IR-corrected potentials at 300 mA/cm^2 in Table S2).

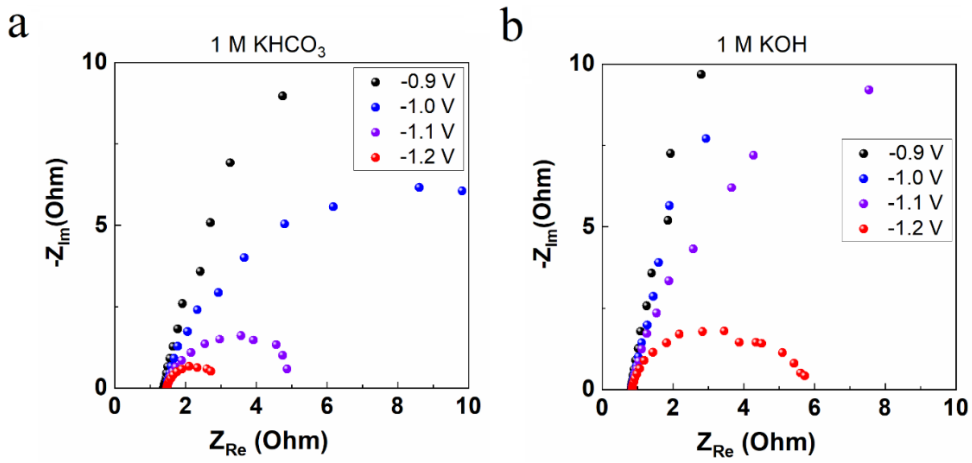

Figure S13. Nyquist plots of Cu deposited GDE in 1 M $KHCO_3$ aqueous solution (a) and 1 M KOH aqueous solution (b) at various potentials.

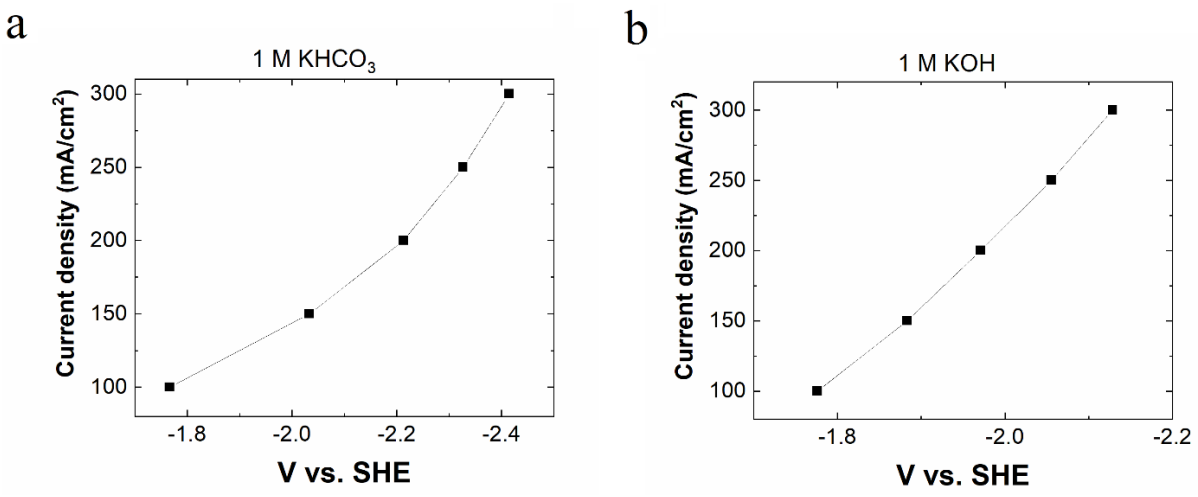

Figure S14. Current densities as a function of potential in 1 M $KHCO_3$ aqueous solution (a) and 1 M KOH aqueous solution (b) (The potentials were not IR-corrected).

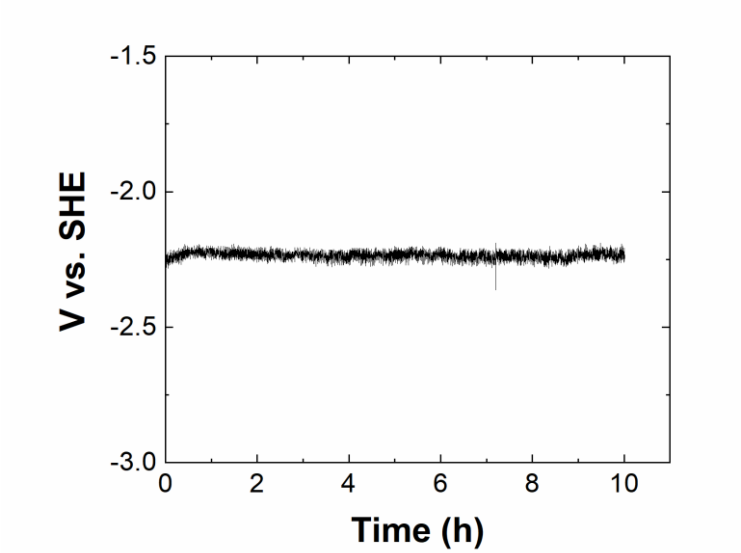

Figure S15. Applied potentials as a function of time at 200 mA/cm^2 in 1 M $KHCO_3$ electrolyte.

Table S1. IR-corrected potentials in 1 M KOH

Current (mA)	R (Ω)	Corrected V vs. SHE
200	0.82	-1.61238
300	0.82	-1.6375
400	0.82	-1.64313
500	0.82	-1.6455
600	0.82	-1.648

Table S2. IR-corrected potentials in 1 M $KHCO_3$.

Current (mA)	R (Ω)	Corrected V vs. SHE
200	1.38	-1.535
300	1.38	-1.6075
400	1.38	-1.63
500	1.38	-1.6425
600	1.38	-1.595

Liquid products

After completion of CO_2 reduction electrolysis (not in-situ analysis), liquid-phase products were analyzed by a high-performance liquid chromatography. In this work, both catholyte and anolyte in the given reservoirs were collected for quantification of liquid products due to that a part of liquid products transported from catholyte to anolyte via AEM (Figure S16). Here, the crossover ratio of one certain liquid product formed on cathode via AEM can be calculated according to the below equation:

$$Crossover\ ratio\ (\%) = \frac{N_{liquid\ in\ anolyte}}{N_{liquid\ in\ anolyte} + N_{liquid\ in\ catholyte}} \times 100\% \qquad (S15)$$

where $N_{liquid\ in\ anolyte}$ and $N_{liquid\ in\ catholyte}$ are the amount of one certain liquid product detected in anolyte and catholyte, respectively. Thus, the above equation can be used to calculate a ratio between the amount of one certain liquid product crossed to anolyte through AEM and the total amount of corresponding liquid product generated on cathode.

It should be noted that the volume of catholyte and anolyte slightly varied after about 2.5 h electrolysis (catholyte volume slightly decreased with increased anolyte), due to the anion species hydrated with water molecules transport from catholyte to anolyte via AEM as charge carriers. Thus, for getting accurate selectivity of liquid products in this study, we also measured volume of catholyte and anolyte after electrolysis, respectively.

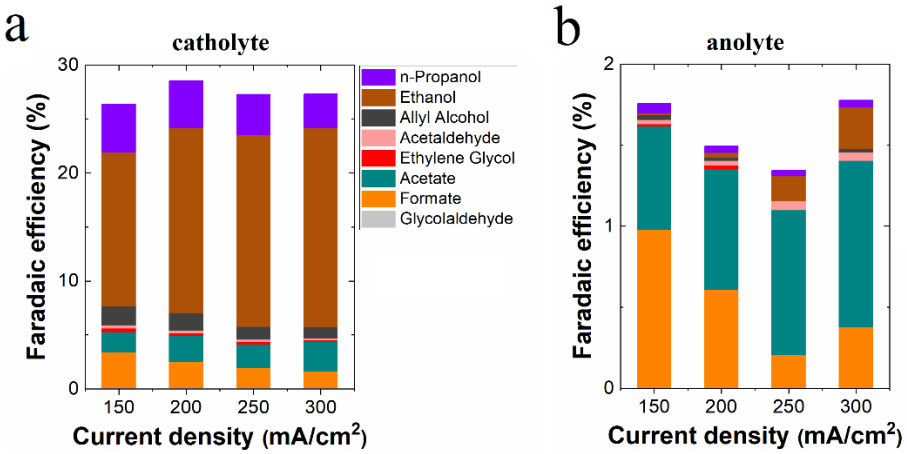

Figure S16. Faradaic efficiencies for all detected liquid products based on catholyte (a) and anolyte (b) in 1 M $KHCO_3$ at various current densities, respectively.

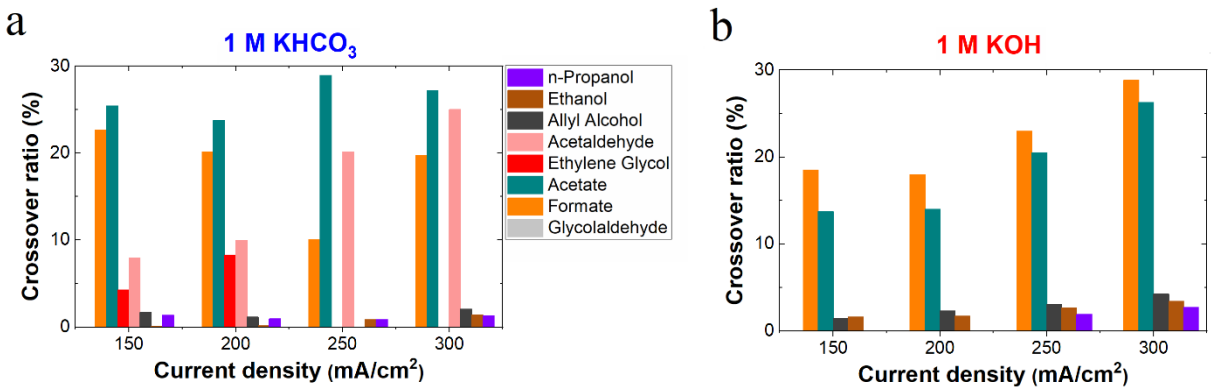

Figure S17. Crossover ratio of liquid products via AEM in 1 M $KHCO_3$ (a) and I M KOH (b) during about 2.5 h CO_2 reduction at various current densities, respectively.

REFERENCES

(1) Kuhl, K. P.; Hatsukade, T.; Cave, E. R.; Abram, D. N.; Kibsgaard, J.; Jaramillo, T. F. Electrocatalytic Conversion of Carbon Dioxide to Methane and Methanol on Transition Metal Surfaces. *Journal of the American Chemical Society* **2014**, *136* (40), 14107–14113. https://doi.org/10.1021/ja505791r.

(2) Hori, Y. Electrochemical CO2 Reduction on Metal Electrodes. In *Modern Aspects of Electrochemistry*; Vayenas, C. G., White, R. E., Gamboa-Aldeco, M. E., E., Ed.; Springer New York: New York, NY, 2004; Vol. 70, pp 89–189. https://doi.org/10.1007/978-0-387-49489-0_3.

(3) Ma, M.; Djanashvili, K.; Smith, W. A. Controllable Hydrocarbon Formation from the Electrochemical Reduction of CO 2 over Cu Nanowire Arrays. *Angewandte Chemie International Edition* **2016**, *55* (23), 6680–6684. https://doi.org/10.1002/anie.201601282.

(4) Kibria, M. G.; Dinh, C. T.; Seifitokaldani, A.; De Luna, P.; Burdyny, T.; Quintero-Bermudez, R.; Ross, M. B.; Bushuyev, O. S.; García de Arquer, F. P.; Yang, P.; et al. A Surface Reconstruction Route to High Productivity and Selectivity in CO 2 Electroreduction toward C 2+ Hydrocarbons. *Advanced Materials* **2018**, *30* (49), 1–7. https://doi.org/10.1002/adma.201804867.